



Decadal variability of tropical Indian Ocean sea surface temperature and its impact on the Indian summer monsoon

Amol Vibhute^{1,2} · Subrota Halder^{1,2} · Prem Singh¹ · Anant Parekh¹ · Jasti S. Chowdary¹ · C. Gnanaseelan¹

Received: 12 September 2019 / Accepted: 2 April 2020 / Published online: 5 May 2020
© Springer-Verlag GmbH Austria, part of Springer Nature 2020

Abstract

Decadal variability of climate over the Pacific and Atlantic Ocean is well studied. However, the decadal climate variability over the Indian Ocean and its possible impact on the summer monsoon received relatively less attention. The present study aims to explore the decadal variability of the Tropical Indian Ocean (TIO) sea surface temperature (SST) and its associations with the Indian summer monsoon rainfall (ISMR) variability. More than a hundred years of observed monthly SST data from Extended Reconstructed sea surface temperature and rainfall data from India Meteorological Department are used for the analysis. In addition to these, century reanalysis fields of winds, moisture, vertical velocity, tropospheric temperature, and sea level pressure are used for diagnosing different processes. Time series and wavelet analysis confirmed the presence of decadal variability (~9 to 30 years) in the TIO SST. The decadal variance of TIO SST is maximum in the eastern equatorial Indian Ocean, followed by the north Arabian Sea. Decadal EOF of TIO SST shows a dominant basin-wide mode explaining about 50% of total variance and has robust decadal variability during 1940 to 1952; wavelet analysis supported this robust signal statistically. Similar analysis for the ISMR reveals that the decadal variance of rainfall has significant strength over monsoon core zone and Western Ghats. The EOF analysis further confirms this spatial pattern of rainfall decadal variability over India. Correlation between decadal TIO SST and over monsoon core zone (MCZ) rainfall is significant with 2 years lag. To understand how the decadal variability of TIO SST influences the ISMR, monsoon features during strong warm and cold phase are studied. During the warm phase, MCZ and Western Ghats receive more rain than normal and vice versa for cold phase. Which is consistent with strong southwesterly winds, strong pressure gradient, and strong convergence over the MCZ for the warm phase. Also, during the warm phase, positive anomaly of mid-troposphere temperature, vertical velocity, and moist static energy are found to be associated with excess convective activity. Apart from this, larger scale zonal (Walker) and meridional (Hadley) circulation fields are also in phase with the TIO SST and rainfall variability. Our study advocates that decadal variability in TIO SST influences the monsoon dynamics and moist thermodynamics leading to near in-phase changes in the rainfall over the MCZ and Western Ghats region.

1 Introduction

Variability is an inherent property of the climate system. It fluctuates at different time scales ranging from days to decades, and it is driven by the internal and external forcing. Understanding decadal climate variability is a prerequisite of current climate research since knowledge about decadal variability is very important in decision-making for planners and

policy makers (e.g., Meehl et al. 2009). The natural internally forced decadal variability has large uncertainty compared to externally forced, and related understanding of natural internal decadal variability is meager (Hawkins and Sutton 2009 and Liu 2012). Internal decadal variability is largely controlled by the oceans because of their thermal and dynamical inertia (Cassou et al. 2018). Decadal variations in ocean temperature are manifestations of ocean heat uptake and heat distribution (Yan et al. 2016). Significant low-frequency variability of sea surface temperature (SST) at decadal and longer time scales reported for the North Pacific (e.g., Trenberth and Hurrell 1994; Nakamura et al. 1997) is known as the “Pacific decadal oscillation” (PDO, Mantua et al. 1997) and decadal variability in the Atlantic Ocean is known as Atlantic multidecadal oscillation (AMO, Schlesinger and Ramankutty 1994). SST anomalies associated with the PDO exhibit a basin-wide horseshoe-

✉ Anant Parekh
anant@tropmet.res.in

¹ Indian Institute of Tropical Meteorology, Pune 411008, India

² Department of Atmospheric and Space Sciences, Savitribai Phule Pune University, Pune, India

like spatial pattern with one sign in the central and western north Pacific surrounded by the opposite sign to the north, east, and south (Mantua et al. 1997). Swings in north Atlantic SST are the central feature of AMO, which shows significant regional and global climatic impacts. Another recently reported decadal variability from the Pacific Ocean is interdecadal Pacific oscillation (IPO), which evolves similar to PDO but covers southern hemisphere as well as the northern hemisphere (Salinger et al. 2001). These decadal variabilities in the Pacific and Atlantic Ocean are better studied; however, the decadal variability of the Indian Ocean is a recently reported mode of variability (Li and Han 2015 e.g., Lee and McPhaden 2008; Han et al. 2010; Feng et al. 2010; Han et al. 2014a, b; ; Dong et al. 2016; Krishnamurthy and Krishnamurthy 2016). It has a basin-wide warming/cooling pattern; Han et al. (2014b) addressed it as the “decadal Indian Ocean Basin (IOB) mode.” Dong and McPhaden (2016) showed that IOB mode is robust in various observational datasets such as Hadley Centre Global Sea Ice and Sea Surface Temperature (HadISST), Extended Reconstructed SST (ERSST), and Kaplan SST. Before 1985, IOB mode was dominated by IPO, but after 1985, due to excess anthropogenic forcing, IOB and IPO are found to be out of phase. The out-of-phase relationship between Indian Ocean and IPO found to be closely linked to the recent shift in the Indian Ocean forcing from a multidecadal to decadal nature (e.g., Mohapatra et al. 2020). According to Li et al. (2015a, b), IOB mode offers climate predictability for the Indian Ocean and surrounding countries; however, the equatorial wind bias in climate models reduces the IOB amplitude and possibly limiting the models’ skill of regional climate prediction. Huang et al. (2019) found that the amplitude of the IOB mode is a seasonally evolving feature, which has strong intensity in early boreal spring compared to other seasons. Another coupled model-based study by Tozuka et al. (2007) found two leading EOFs for TIO SST decadal variability, a basin-wide decadal mode, and a decadal dipole mode. Studies by Wang and Mehta (2008) and Bader and Latif (2005) noted that the low-frequency variability of Indian Ocean SST can influence the tropical and extra-tropical atmosphere via changes in the Walker and Hadley circulations.

The interannual variability in Indian summer monsoon rainfall (ISMR) is explored extensively in the past and mostly linked with TIO and Pacific SST variability, El Niño Southern Oscillation (ENSO), and equatorial Indian Ocean SST Oscillations, which are two critical modes of SST for interannual monsoon variability (e.g., Goswami 2006, Gadgil et al. 2007). Xavier et al. (2007) found that the ENSO influences interannual variability in ISMR by modulating the length of the monsoon season. Fasullo (2004) brought out strong correspondence between the ISMR and ENSO biennial variability spectral and spatial characteristics. Yoo et al. (2006) revealed that the TIO SST basin mode with maximum variance in the

southern hemisphere has larger impact on south Asian monsoon variability than the Indian Ocean Dipole. From the AMIP experiments, Cherchi and Navarra (2013)) found that the interannual variability of all the monsoon indices are forced by the SST but different SST conditions in the Indo-Pacific sector may provide similar monsoon characteristics over India, reflecting the complexity of the relationship between ENSO, Indian Ocean SST, and the monsoon, an influence from other oceanic sectors rather than from the Indian-Pacific alone. Goswami et al. (2006) revealed that the North Atlantic Oscillation-associated storm-track changes during northern summer affects troposphere temperature over southern Eurasia, and can modulate the ISMR. Moreover, coupled models have displayed reasonable skill in the prediction of ISMR variability (Rajeevan et al. 2012), where local and global tropical ocean air-sea coupling representation is vital for better skill of the coupled models (Koul et al. 2018).

Moreover, some studies have shown that the ISMR exhibits decadal variability with alternate epochs of above-normal and below-normal rainfall (Kripalani and Kulkarni 1997a; Kripalani and Kulkarni 1997b; Mehta and Lau 1997; Krishnamurthy and Goswami 2000). Pant et al. (1988) revealed that the low-frequency climate variations have contributed to the instability of the correlations of ISMR with predictors. Kripalani and Kulkarni (1997b) reported that the impact of El Niño (La Niña) is dependent on the phase of low-frequency ISMR epoch. Using wavelet analysis, Torrence and Webster (1999) found that the ENSO and ISMR had experienced interdecadal variability over the last 125 years on a 12–20-year timescale. Moreover, Krishnamurthy and Goswami (2000) found that the decadal ENSO variability modulates the interannual ENSO-monsoon relation. Krishnan and Sugi (2003) found similar relation between the equatorial Pacific SST and the Indian monsoon in both the decadal and interannual ENSO monsoon rainfall relation. From wavelet decomposition of ISMR and Niño-3 SST over the past 50 years, Fasullo (2004) revealed that the strong correspondence exists between the low-frequency evolution of biennial power in them. Yoo et al. (2006) recommended that more studies with longer data records and reliable models are necessary to bring out the leading mechanisms responsible for the SST’s impact on the monsoon, which is not yet fully understood. Sen Roy (2011a) and Roy and Sen Roy (2011) reported that the positive phase of the PDO resulted in a general persistence of droughts and dry years, with slightly stronger impact during El Niño years, while, during the negative phase of PDO, the El Niño effects became more prominent in the form of distinctly dry years interspersed with normal or above-normal wet years. Previous studies have also shown considerable decadal variability in the presence of the biennial oscillation (e.g., Li et al. 2012). Izumo et al. (2014) proposed that the Indian Ocean Dipole-ENSO interactions favor a biennial time scale and interact with the slower recharge-

discharge cycle intrinsic to the Pacific Ocean. Using long observed ISMR data and coupled model simulations, a recent study (Krishnamurthy and Krishnamurthy 2014) has shown that the PDO influences the variability of ISMR and monsoon-ENSO relation. ISMR is closely coupled with the Indian Ocean, which enhances the possibility of decadal variability in Indian Ocean SST (Han et al. 2014b) influencing ISMR variability. Ashok et al. (2004) found that there are strong decadal Indian Ocean Dipole events associated with thermocline variability in TIO through zonal wind forcing. This decadal variability of Indian Ocean dipole is independent of ENSO decadal variability. Li et al. (2016a, b) found that the projected Indian Ocean dipole-like pattern of mean changes and frequency increase of extreme positive Indian Ocean dipole events are largely the artifacts of model errors and unlikely to emerge in the future. However, previous attempts have failed to provide a comprehensive picture of the temporal variability of the monsoon rainfall on decadal time scale (e.g., Sen Roy et al. 2003; Sen Roy 2011b) and their linkage with TIO SST. This has motivated us to explore the temporal and spatial features of decadal variability in TIO SST and ISMR and their linkages. Summer monsoon features during strongest warm/cold phase of TIO SST mode is also studied in detail. This study may help for the development of decadal prediction of monsoon, which is a prerequisite for long-term planning. Section 2 discusses data and methodology used in the study, results and discussion are provided in Section 3, and Section 4 is the summary and conclusion.

2 Data used and methodology

2.1 SST data

SST is one of the most important indicators of climate variability, which is used widely to identify the decadal variability. The ERSST dataset is a global monthly SST dataset derived from the International Comprehensive Ocean–Atmosphere Dataset. It is produced on a $2^\circ \times 2^\circ$ grid with spatial completeness enhanced using statistical methods. This monthly analysis begins in January 1854, and continues to the present. The latest version of ERSST, version 4, is based on optimally tuned parameters using the latest datasets with improved analysis methods (Huang et al. 2014; Liu et al. 2014; Huang et al. 2015). This monthly data is converted to annual mean (from year 1854 to 2016) for present study. Apart from this, the Met Office Hadley Centre's sea ice and SST data set, HadISST, replaces the Global Sea Ice and Sea Surface Temperature (GISST) data sets and is a unique combination of monthly globally complete fields of SST and sea ice concentration on a $1^\circ \times 1^\circ$ grid. HadISST temperature data was reconstructed using a two-stage reduced-space optimal interpolation procedure, followed by superposition of quality-improved gridded observations onto the

reconstructions to restore local details. We used this monthly data from 1870 to 2016 for the present study.

2.2 Rainfall data

India Meteorological Department has brought out a high-resolution daily gridded rainfall data set for the period 1900–2016 (Rajeevan et al. 2006; Pai et al. 2014) using stations' observations. This dataset is widely used for many monsoon-related studies (e.g., Goswami et al. 2006; Krishnamurthy and Shukla 2008; Ajaymohan and Rao 2008; Konwar et al. 2012). This dataset has considered stations which had a minimum 70% data availability during the analysis period in order to minimize the risk of generating temporal inhomogeneities in the gridded data due to varying station densities. Since the present analysis uses a fixed rainfall network, it is used for examining long-term rainfall climate variability like decadal variability. This daily data is averaged for summer monsoon (June to September) to get seasonal mean data for this study. For two regions, all India (considered ISMR) as well as for the monsoon core zone (MCZ, Rajeevan et al. 2010, Mandke et al. 2007), this dataset is analyzed; Fig. 3b displays the MCZ region. The interannual variation of the ISMR is highly correlated (0.91) with that of the summer monsoon rainfall over the MCZ, suggesting that it is a critical region for the interannual variation of rainfall.

2.3 ERA-20C reanalysis data

ERA-20C is European Center for Medium Range Weather Forecast first atmospheric reanalysis of the twentieth century, from 1900 to 2010 (Poli et al. 2016). It is an outcome of the ERA-CLIM project. Many other reanalysis, such as NCEP reanalysis-1 (available from 1948 to present) and NCEP reanalysis-2 (available from 1979 to present), ERA-Interim and ERA5 (available from 1979), are widely used reanalysis but not available for the entire study period. But ERA-20C covers the present study period and it is considered one of the state-of-the-art century reanalysis data (Poli et al. 2016). The observations assimilated in ERA-20C include surface and mean sea level pressures from International Surface Pressure Databank (ISPDv3.2.6) and surface marine winds from International Comprehensive Ocean–Atmosphere Dataset v2.5.1. The assimilation methodology is a 24-h 4D-Var analysis, with variational bias correction of surface pressure observations. The analyses provide the initial conditions for subsequent forecasts that serve as backgrounds to the next analyses. The ERA-20C reanalysis was produced with Integrated Forecasting System version Cy38r1 and the same surface and atmospheric forcing as the final version of the atmospheric model integration. A coupled atmosphere/land-surface/ocean-waves model is used to reanalyze the weather, by assimilating surface observations. The ERA-20C products

describe the spatial-temporal evolution of the atmosphere (on 91 vertical levels, between the surface and 0.01 hPa), the land-surface (on four soil layers), and the ocean waves (on 25 frequencies and 12 directions). To understand corresponding changes in the monsoon features (i.e., troposphere temperature, integrated troposphere moisture and its transport, vertical moist thermodynamic structure, spatial distribution of sea level pressure, and moist static energy) during the phases of decadal variability, temperature, winds, specific humidity, sea level pressure, and vertical velocity data from ERA-20C are used.

2.4 Methodology

To carry out various analysis, TIO SST monthly data are de-trended and annually averaged, and rainfall, moisture, winds, and temperature are averaged for the summer monsoon season (June to September). To identify dominant variability in TIO SST and ISMR, techniques such as spectrum analysis, wavelet analysis are used. Spectrum analysis gives dominant signal within the whole time series, whereas wavelet analysis provides more accurately localized temporal and frequency information. This allows detailed analysis of time-dependent signal characteristics. Here Morlet wavelet function is used for the wavelet analysis. It is being a complex function, and allows detection of both the time-dependent amplitude and the phase (Torrence and Compo 1998). In addition, wavelet analysis can reveal whether the variability has significant strength or not; in this study, decadal variability for TIO SST and ISMR was identified through wavelet analysis with qualified confidence level of 80%. In addition, coherent wavelet analysis is carried out between the TIO SST and ISMR/MCZ rainfall for the common period of 1901–2016. It shows strong coherence for the decadal scale during 1930–1960. To extract the identified dominant variability signal (i.e., decadal signal), band-pass filtering is applied on the TIO SST and ISMR time series data. Band-pass filter retains interested variability signal and eliminates other variability signal. According to wavelet/spectrum peak for decadal signal, higher cutoff frequency for band-pass filtering of 0.111, and lower cutoff frequency of 0.0333, corresponding to the period of 9 to 30 years, is considered. The filtering exercise facilitates to exclusively study temporal and spatial scales of decadal variability. To get the dominant spatial modes of identified decadal variability, empirical orthogonal function (EOF) analysis is carried out on the filtered TIO SST and ISMR data. To know the coherence between the dominant decadal variability signal of TIO SST and ISMR, with the decadal modes (e.g., PDO, AMO, IPO), correlation coefficient is estimated with respective indices of decadal modes. The difference of SST anomaly averaged over the central equatorial Pacific, and in the northwest and southwest Pacific (Salinger et al. 2001) is called the IPO index.

According to Trenberth and Shea (2006), AMO index is defined as the de-trended 10-year low-pass filtered annual mean area-averaged SST anomaly over the north Atlantic basin (0° N–65° N, 80° W–0° E). To know the lead/lag relation between TIO SST/ISMR decadal variability, cross-correlation analysis is carried out. Student's *t* test is used to know whether correlation between the two decadal variability is significant or not. The ISMR is calculated over all Indian region and MCZ rainfall is calculated over MCZ.

During the strong phases of TIO SST, variability in monsoon features are studied using ERA-20C reanalysis data of sea level pressure, low-level and upper level monsoon winds, vertically integrated moisture transport, and tropospheric temperature. In addition, monsoon-associated zonal and meridional circulation cells are studied, zonal cell over the region 40° E to 120° E averaged between 18° N and 28° N, and meridional cell over the region 20° S to 40° N averaged between 70° E and 90° E are examined. Corresponding response of tropospheric temperature is also studied for the warm and cold phases, and troposphere temperature anomaly is computed using temperature data between 600 and 200 hPa following Xavier et al. (2007). The vertically integrated moisture transport (VIMT, gm/m/s) is also estimated using specific humidity, *u*, and *v* components of wind integrated from 1000 hPa to 300 hPa as in Konwar et al. (2012). Besides, vertical structure of winds, temperature, moisture, and moist static energy (MSE) is studied over the MCZ associated with the warm and cold phases of decadal variability. MSE is diagnostic to identify leading moist and radiative processes deemed responsible for rainfall anomalies over mean ascent regions (Su and Neelin 2002; Maloney 2009; Annamalai 2010).

The moist static energy is estimated by

$$\text{MSE} = (c_p \times T) + (g \times z) + (L \times q) \quad (1)$$

where *T* is the temperature, *c_p* is the specific heat of air at constant pressure, *g* is the acceleration due to gravity, *z* is the height, *L* is the latent heat of evaporation, and *q* is the specific humidity. The physical meaning of this definition of MSE is relatively intuitive: the first term is the dry-air enthalpy (or “heat content”), the second term is the specific gravitational potential energy, and the last term is the potential contribution to the first term due to latent heating. It is also intuitively expected that the sum of these three terms is conserved under adiabatic and hydrostatic transformations.

3 Result and discussion

3.1 Temporal and spatial evolution of TIO SST and summer monsoon rainfall variability

Figure 1a and b show the time series of de-trended TIO SST anomalies and summer monsoon rainfall anomalies (ISMR

and MCZ rainfall) during the study period. From the time series analysis, it is found that there are aperiodic oscillations in the time series of de-trended SST anomaly (Fig. 1a). This analysis also confirms that ERSST and HadISST are consistent with each other for TIO SST anomaly evolution during the study period, where the correlation coefficient between them is 0.9, which confirms the robustness of the TIO SST data; hence, the rest of the study used ERSST for further analysis. In case of rainfall time series, all India and MCZ display correlation coefficient of 0.84 between them, indicating high level of coherence, which is consistent with the findings of Rajeevan et al. (2010). Figure 1c and d show the wavelet analysis of SST and ISMR, in which the x -axis is the time, the y -axis is the period, and contours show the strength of the signal. Contour under the thick black line displays signal with 80% confidence level, and right panels show the power spectrum. The significant peak at about the period of 20 years in the power spectra of TIO SST (Fig. 1c) indicates the decadal variability with the spread of 12–30 years, which has significant power during 1910 to 1970. Such a decadal variability of SST and coherent changes in the atmospheric parameters are reported (surface winds, sea level pressure, cloud) in the southern Indian Ocean (Allan et al. 1995). Figure 1d shows the decadal variability (about 17 years) in the rainfall over the Indian region, which was strongest during 1935 to 2000. It also shows that the decadal variability has spread from 09 to 30 years. To eliminate all other variabilities and to retain only decadal variability, band-pass filter is applied to time series of de-trended TIO SST and rainfall anomaly of 9–30 years. By analysis of 108 years of summer monsoon, rainfall data over India Mooley and Parthasarathy (1984) found two cycles 14 years and 28 years but were not consistent throughout the period. They also found that 14-year cycle was prominent during the 1925–1978 period. Using wavelet analysis, Torrence and Compo (1998) found that the ISMR and ENSO indices exhibited high coherence during 1875–1920 and 1960–1990, but low coherence during 1920–1960.

Figure 2(a) shows the band-pass filtered time series of TIO SST anomaly, MCZ rainfall anomaly, and AMO index. Filtered TIO SST anomaly displays a range of -0.20 to 0.36 °C. A strong positive phase is found during 1940 to 1945 (warm phase) with the amplitude of 0.36 °C and followed by negative phase with strength of -0.2 °C (cold phase). AMO displays an amplitude range of -0.18 to 0.18 °C and correlates with TIO SST ($r=0.36$). This qualitative analysis indicates that the strength of decadal variability of TIO SST is higher than AMO index. Over the MCZ rainfall also shows decadal variability, which has an amplitude of 2.5 to 3 mm/day; however, for the ISMR, it is 0.6 mm/day. TIO SST displays weak (0.2) simultaneous correlation with MCZ rainfall for decadal variability; however, it shows 0.6 correlation with the lag of 2 years. Hence, TIO SST and MCZ rainfall decadal

variability are very closely in phase though with some lag. Figure 2(b) shows the band-pass filtered time series of TIO SST, PDO, and IPO Index during 1860 to 2016. PDO and IPO indices display significant correlation with TIO SST (0.26 and 0.29 respectively) but lesser than with AMO for the study period. Li et al. (2016a, b) and Kucharski et al. (2016) suggested that the positive AMO favors the basin-wide warm SST anomalies in the TIO. Zhou et al. (2015) suggested that a positive-phase AMO can lead to an Indo-Pacific warm SST response. However, the contribution of the AMO to the interdecadal Indian Ocean basin mode remains unclear. Krishnan and Sugi (2003) found that warm (cold) phase of the PDO decreases (increases) the monsoon rainfall and increases (decreases) the surface air temperature over the Indian subcontinent. Li et al. (2017) conclude that an improved simulation of western Pacific convection is a priority for reliable ISMR projections in coupled models. Dong and McPhaden (2017) reported that the relationship between TIO SST and Pacific basins underwent a dramatic transformation beginning around 1985. Before that, SST variations associated with the Indian Ocean basin and the IPO were positively correlated, whereas afterward they were much less synchronized. Thus, IPO and TIO SST show in-phase and out-of-phase relationship in a specific period, out-of-phase relationship up to the year 1940 having correlation coefficient -0.56 and after 1990 having -0.7 . In-phase relationship from 1940 to 1990 with correlation of 0.6 having a strongly positive phase about the years 1945 and 1960. The above discussion directs that TIO and Pacific SSTs do not retain in phase relation, and vary over the study period.

It is important to note that time series analysis shows that during 1940 to 1990, TIO SST and MCZ rainfall are in phase, whereas during the 1990 to 2016 and 1900 to 1940 it shows mostly out of phase. Overall, the analysis reveals that on decadal scale, TIO SST and MCZ rainfall have strong in-phase relation with some phase lag followed by the relation with AMO, PDO, and IPO during 1940 to 1990. This analysis indicates that TIO SST decadal variability may have close association with the monsoon rainfall over the core region. Some studies have suggested an increase in moisture availability and land–sea thermal gradient in the tropics due to warming phase, favoring an increase in tropical rainfall (e.g., Kamae et al. 2014). The remote influence of the Pacific interdecadal variability on the monsoon is associated with prominent signals in the tropical and southern Indian Ocean indicative of coherent inter-basin variability on decadal time scales (Krishnan and Sugi 2003). Hence, the TIO SST and monsoon rainfall decadal variability spatial features are explored in the next section.

Figure 3a shows the spatial distribution of the TIO SST variance for decadal variability. It shows high variance to the south eastern part of Indian Ocean and north of Arabian Sea, moderate variance to the eastern part of Bay of Bengal, and

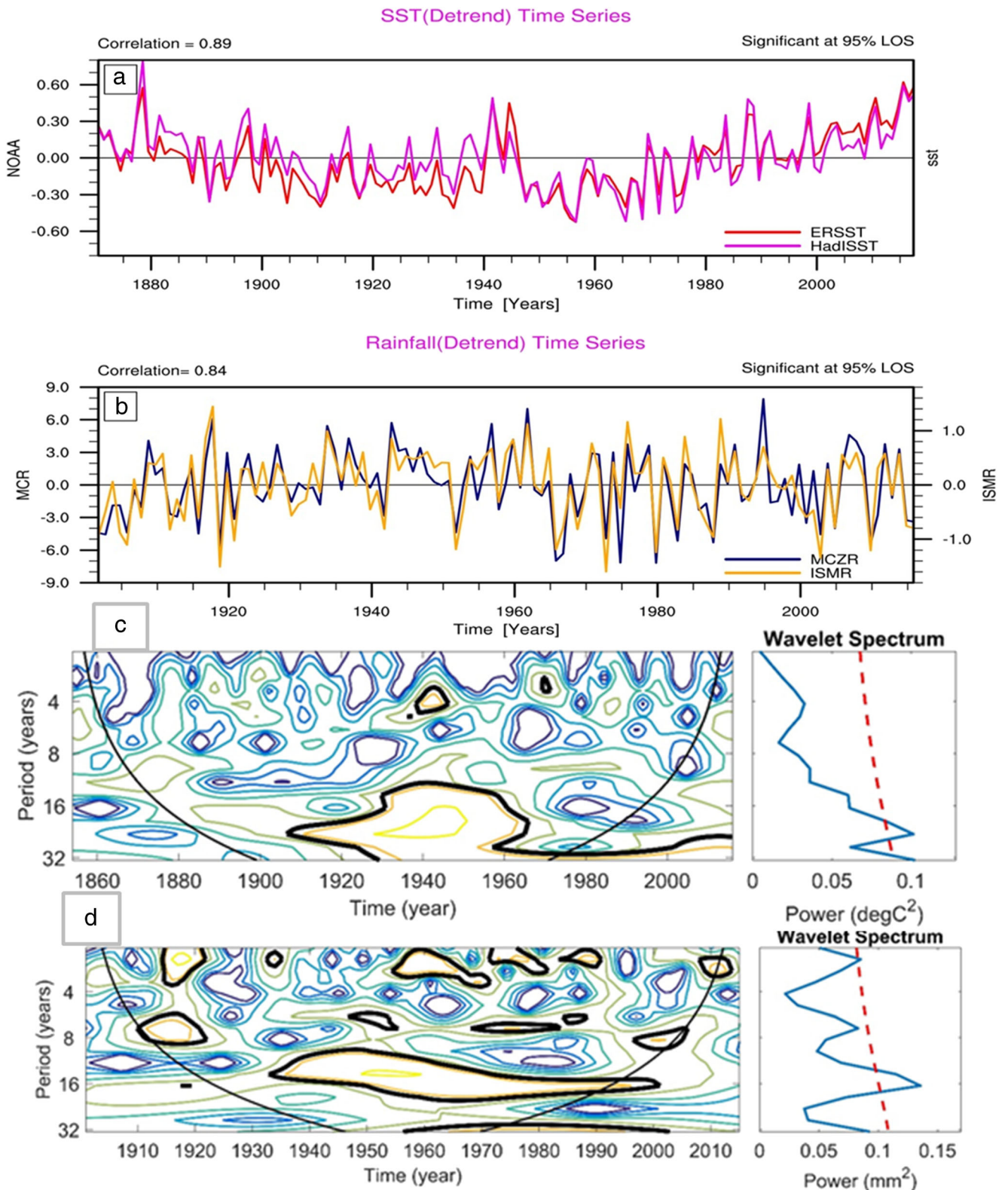


Fig. 1 Time series of de-trended **a** annual SST anomaly ($^{\circ}\text{C}$) of the TIO from ERSST and HadISST and **b** ISMR and MCZR rainfall anomaly (mm/day), corresponding wavelet analysis and power spectrum analysis of **c** TIO SST from ERSST, and **d** ISMR (JJAS) from IMD data. Where contour with thick black line qualifies as the 80% confidence level, while in power spectrum red line is white noise spectrum for 80% confidence level

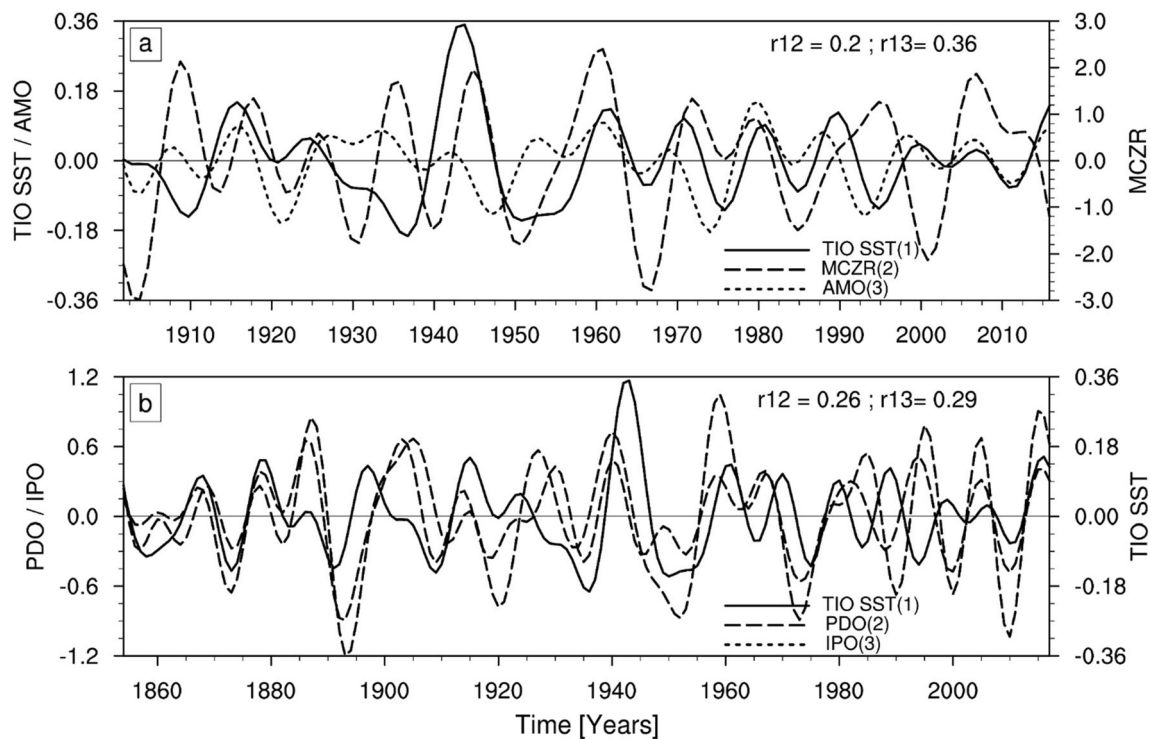


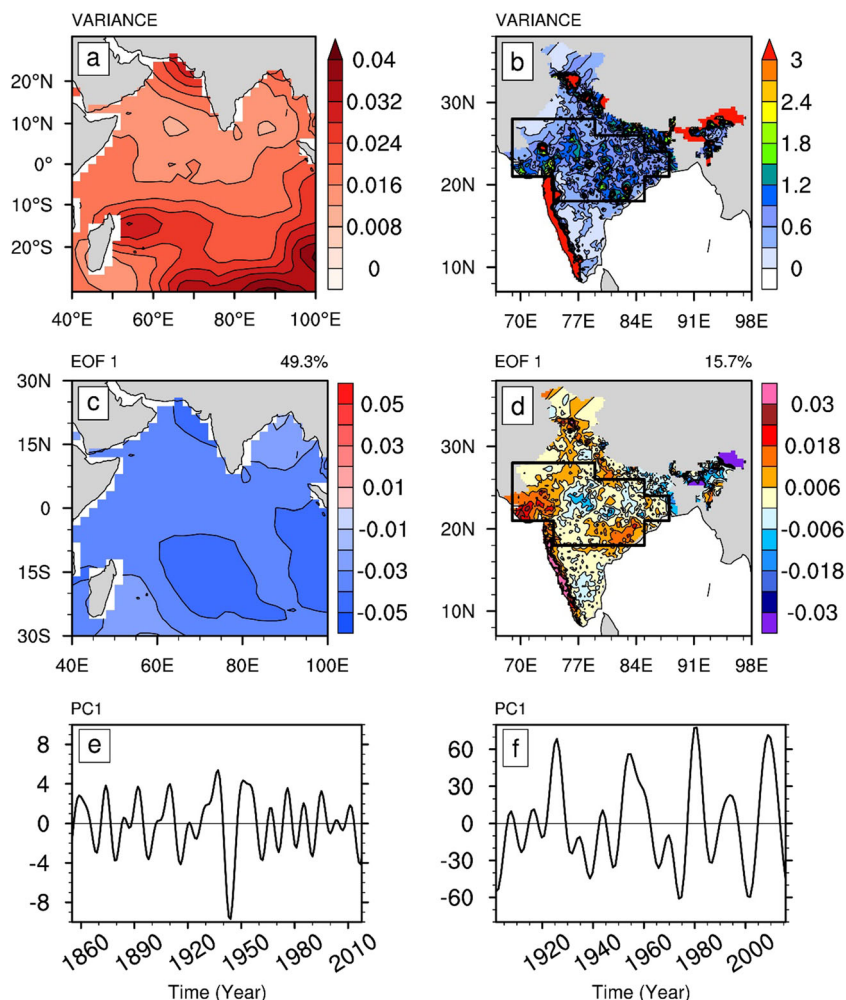
Fig. 2 Band-pass filtered (9 to 30 years) time series of (a) TIOSST, MCZ rainfall, and AMO Index from year 1901 to 2016 and (b) TIOSST, PDO, and IPO Index from year 1854 to 2016 and correlation between them mentioned in upper right hand side corner

low variance in the central and western part of Indian Ocean. However, rainfall (Fig. 3b) shows high variance over the Western Ghats, north east India, and some part of foot hills of Himalaya and the MCZ and low variance over the rest of India. To identify the spatial pattern of decadal variability, EOF analysis is carried out on the band-pass filtered SST and rainfall anomalies. Figure 3c shows the first mode of decadal variability in TIO SST during the study period (i.e., 1854 to 2016). The first mode of EOF is basin-wide mode explaining 49.3% of total variance. These results are consistent with Han et al. (2014b), who identified this mode as IOB mode. The second mode is dipole-like mode explaining 10.6% of total variance. Dong and McPhaden (2017) carried out similar analysis with three different 13-year low-pass filtered annual mean SSTs (i.e., ERSST, HadISST, and Kaplan SST) and found similar IOB mode. However, variance of first mode is slightly higher, which may be due to the use of 13-year low-pass filter. The first mode of TIO SST decadal variability has higher variance in the east equatorial Indian Ocean, the south Indian Ocean, and the north Arabian Sea; however, relatively lesser variance is found in the northern Bay of Bengal and east of Madagascar bay. Figure 3d shows the first mode of ISMR decadal variability during 1900 to 2016 over the India. The first mode explains about 16% of the total variance and has positive phase almost over India (strong signal is reported over the Western Ghats, central India, western and northern India). Figure 3e and f show the

respective principal components for the first mode of SST and rainfall. Principal components (Fig. 3e) of filtered SST anomaly, as well as wavelet analysis, confirmed that first mode was strongest during 1940 to 1960. This dominant mode supports that decadal mode of rainfall also has significant variability during the same period, which is higher in the MCZ and the Western Ghats region.

Figure 4(a, b) displays the spatial patterns of SST anomaly during the warm (1940 to 1945), and cold (1948 to 1952) epochs and the differences are shown in Fig. 4(c). It shows basin-wide warming (except north Bay of Bengal) by 0.2 to 0.3 °C during positive epoch and basin-wide cooling of 0.2 to 0.5 °C during negative epoch. These warming and cooling cycle of TIO SST can affect the monsoon circulation by modifying the zonal circulation (Luo et al. 2012). The spatial pattern and strength of TIO SST play important role in determining the location of precipitation in the monsoon regions (Lindzen and Nigam 1987). From cross-correlation analysis, it is found that TIO SST and MCZ rainfall have significant correlation (0.6) at a lag of 2 years, which is the reason behind the rainfall epoch selection of 1942 to 1947 and 1950 to 1954 (Fig. 4(d, e)). For the warm phase of TIOSST, strong positive rainfall anomalies are found in MCZ and along the Western Ghats. Figure 4(f) shows the difference of summer rainfall between warm phase and cold phase, indicating strong rainfall difference of 3 to 4 mm/day over MCZ and Western Ghats, which supports higher rain during the warm epoch of TIO

Fig. 3 Variance of decadal variability of **a** TIO SST ($^{\circ}\text{C}$)² and **b** ISMR(mm/day)², **c** EOF first mode of TIO SST ($^{\circ}\text{C}$) decadal variability, and **d** EOF first mode of ISMR (mm/day) decadal variability and corresponding principal components are shown in **e** and **f**. The box displayed in **b** and **d** represents the MCZ region

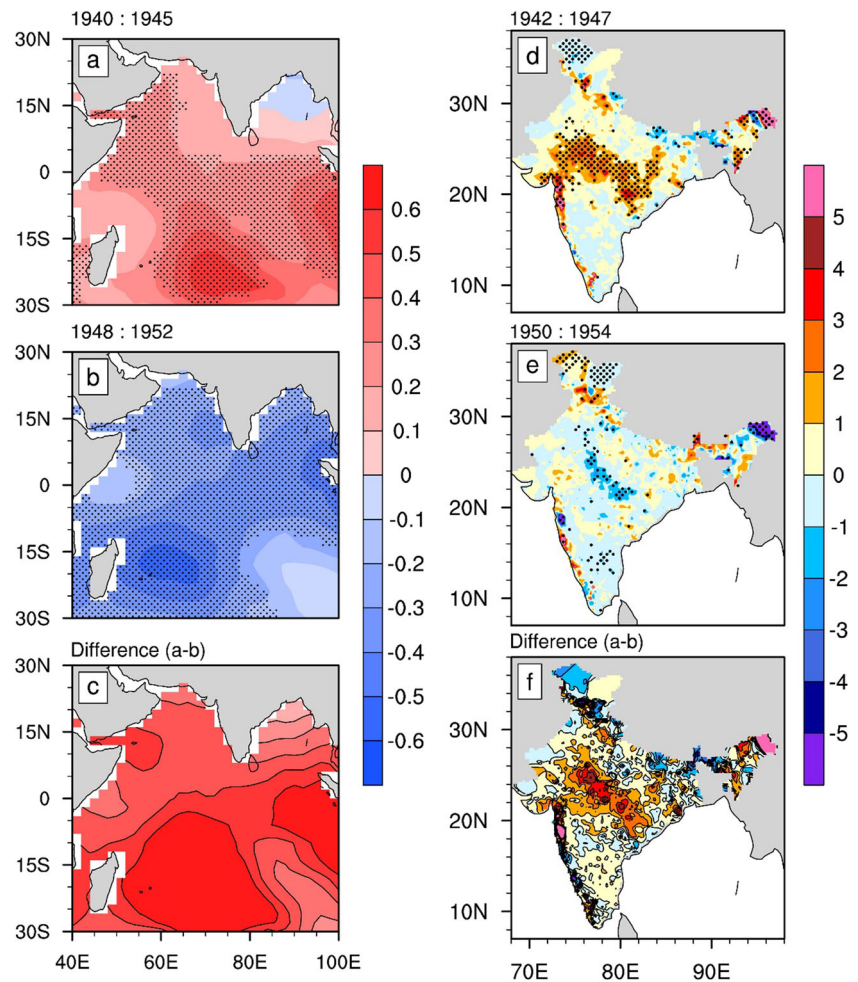


SST decadal variability and vice versa for cold epoch. This nature of rainfall raises the question how warming (cooling) in TIO SST supports more (less) rainfall. It is important to note that during 1942–1947, no deficient monsoon years occurred, and in fact 1942 was an excess monsoon rainfall year. In addition to the above, during this period, Niño3.4 remains negative throughout the period, and during 1942 winter strong negative SST anomaly ($-1.5\text{ }^{\circ}\text{C}$) was reported in Niño3.4. However, dipole mode index did not show any specific phase during this period, and it was within the $\pm 0.5\text{ }^{\circ}\text{C}$, whereas during 1950–1954, most of the summer monsoon rainfall was below normal, and in 1951 it was deficit by 18.7%. During this period, 1951 and 1953 were El Niño years, and during 1951, winter Niño3.4 was anomalously warm by $1.2\text{ }^{\circ}\text{C}$. During 1950 to 1954, dipole mode index was negative mostly, indicating negative dipole. To understand further the status of monsoon features, various parameters (lower and upper level winds, sea level pressure, mid-troposphere temperature, integrated moisture, and moisture transport) are studied using ERA-20C reanalysis data with special emphasis given to MCZ.

3.2 Monsoon features during the warm and cold phase of TIO SST decadal variability

Figure 5(a, b) shows summer monsoon averaged wind speed and wind direction anomaly at 850 hPa during warm and cold phases. During the warm phase, the wind speed difference is positive throughout the basin at 850-hPa level (Fig. 5(c)), indicating strong southwesterly winds over the Arabian Sea, over the MCZ, and the Bay of Bengal than cold phase. It also shows that during warm phase, Western Ghats region experiences intense surface westerlies. This flow transports mass and moisture into the monsoon domain and essentially modulates the amount of rainfall. The strong low-level jet supports excess rainfall over the west coast of India (Findlater 1969). Overall, noticeable difference during warm to cold phase in the low-level circulation was reported over the Arabian Sea and MCZ, which is relatively small for the upper level winds. These changes in the low-level winds are consistent with changes in sea level pressure gradient during the respective phases. Figure 5(d–f) shows the anomaly of vertically integrated moisture flux and moisture flux transport during the

Fig. 4 SST anomaly during (a) dominant positive (1940–1945) and (b) negative phase (1948–1952) and (c) difference (a–b) of anomaly and (d, e) spatial pattern of JJAS rainfall (mm/day) anomaly during (d) dominant positive (1942–1947) and (e) negative phase (1950–1954) and (f) difference (d–e) of anomaly. Black dots represent significant values at the 95% confidence

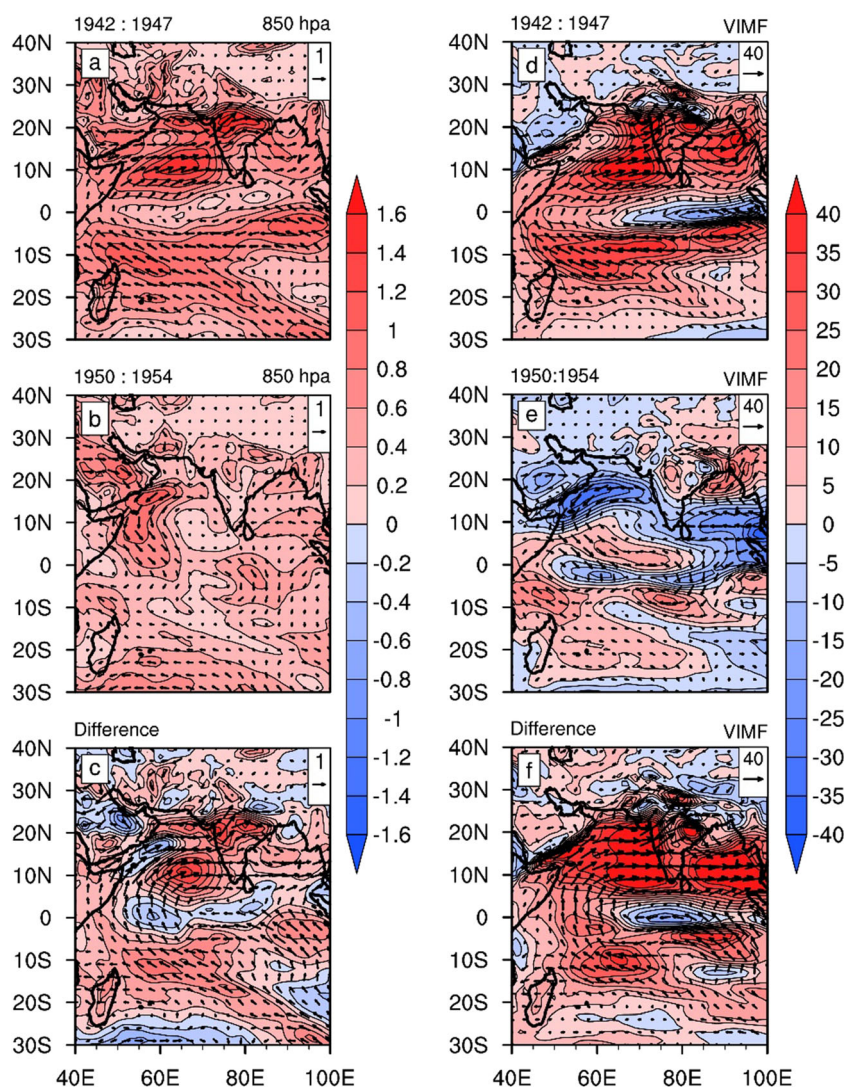


warm and cold phases and their difference. During the warm phase, positive anomaly of moisture flux is present throughout the monsoon flow, including along the Western Ghats, eastern central India, south Indian Ocean, and the Bay of Bengal and negative anomaly of moisture flux over the eastern equatorial Indian Ocean and some part of the monsoon trough region. Vertically integrated moisture transport anomaly is strong easterly south of the equator and westerly north of the equator, which replicate the strong monsoon flow. Convergence of moisture flux is reported along the foothills. This analysis supports that during the warm phase, excess moisture is transported to the monsoon region, which supports the formation of excess precipitation during this phase. During the cold phase, there was negative moisture flux anomaly off Somalia, north Bay of Bengal, along the eastern part of the foot hills, and over the north east region, whereas there was weak positive anomaly over the peninsular India. There was negative anomaly of moisture flux in the eastern Indian Ocean, north Arabian Sea, and some part of central India. Vertically integrated moisture transport displays north easterly anomaly over the Arabian Sea, and northerly transport over the central India. This manifests that during the cold phase, moisture transport

was below normal and supported negative or weak positive anomaly of rainfall over the MCZ, mostly positive anomaly over the oceanic region. Figure 5(f) shows the difference of integrated moisture flux and its transports during the warm and cold phases. Over India, moisture flux anomaly difference has resemblance with rain fall pattern (Fig. 4(d)), which also shows heavy moisture loading along the monsoon flow. The warm phase provides excess moisture, which gets converted in to the excess rainfall over the Western Ghats and MCZ, while during negative phase, weaker transport associated with monsoon leads to weaker monsoon rainfall activity.

High sea level pressure anomaly (Fig. 6(a, b)) is observed over the southern Indian Ocean and decreases as moving towards the central India during both the phases. During the warm phase, Mascarene high has positive sea level pressure anomaly, and monsoon trough region has negative sea level pressure anomaly, whereas during the cold phase, weak anomalies are reported over both regions. This supports that sea level pressure gradient during the warm phase is stronger between the Mascarene high and monsoon trough region than cold phase (Fig. 6(c)), consistent with the low-level wind anomaly during the respective phases. Figure 6(d, e) shows

Fig. 5 Spatial pattern of JJAS Winds anomaly (m/s, shaded is magnitude and vector is direction) from ERA-20C dataset at 850-hPa level composite for (a) warm and (b) cold phase and (c) difference between them. Spatial pattern of JJAS mean vertically integrated moisture flux anomaly (shaded, gm/m/s) and vertically integrated moisture transport anomaly (Vectors, gm/m/s) for (d) warm and (e) cold phase and (f) difference respectively



the troposphere temperature anomaly (averaged over 200 to 600 hPa) for the warm and cold phase, respectively; this troposphere temperature anomaly represents monsoon-associated heating, which has meridional gradient during the summer monsoon. This characteristic of troposphere temperature is crucial to initiate and maintain the large-scale monsoon circulation (Flohn 1957, 1960, Allan et al. 1995, Xavier et al. 2007 and Liu and Yanai 2001) and has coherent variability with the monsoon precipitation (Meehl 1994) on seasonal to interannual scale. Figure 6(d) shows strong positive anomaly of troposphere temperature over Pakistan and adjoining areas; however, over the Tibet and central India, it is less positive during the warm phase, whereas anomaly is weak positive north of 20° N and negative over rest of the study area during the cold phase (Fig. 6(e)). Pattnayak et al. (2016) found that the troposphere temperature over Pakistan better correlates with the ISMR than those over Tibet and Central India. The troposphere temperature anomaly difference (Fig. 6(f)) is positive throughout the study region, corroborating the

strong large-scale monsoon circulation during the warm phase than the cold phase. Corresponding meridional gradient in troposphere temperature is marginally higher in the warm phase than in the cold phase. Besides, areal extent of warm troposphere temperature over the Tibetan region is higher in the warm phase than in the cold phase. These features of troposphere temperature are consistent with the monsoon features during the respective phases. Figure 6(g–i) shows the MSE and MSE anomaly for the warm and cold phases and their difference, respectively. During the warm phase (Fig. 6(g)), positive MSE anomaly is reported over India, with maximum amplitude over the north west India and weak negative anomaly reported over the Arabian Sea and south eastern Indian ocean, whereas during the cold phase most of the area is covered by the negative MSE anomaly (Fig. 6(h)), except over the Tibetan region. This analysis reveals that warm phase favors above-normal MSE over the monsoon domain, favorable for unstable boundary layer, convective ascent, and support excess rainfall (e.g., Raju et al. 2018).

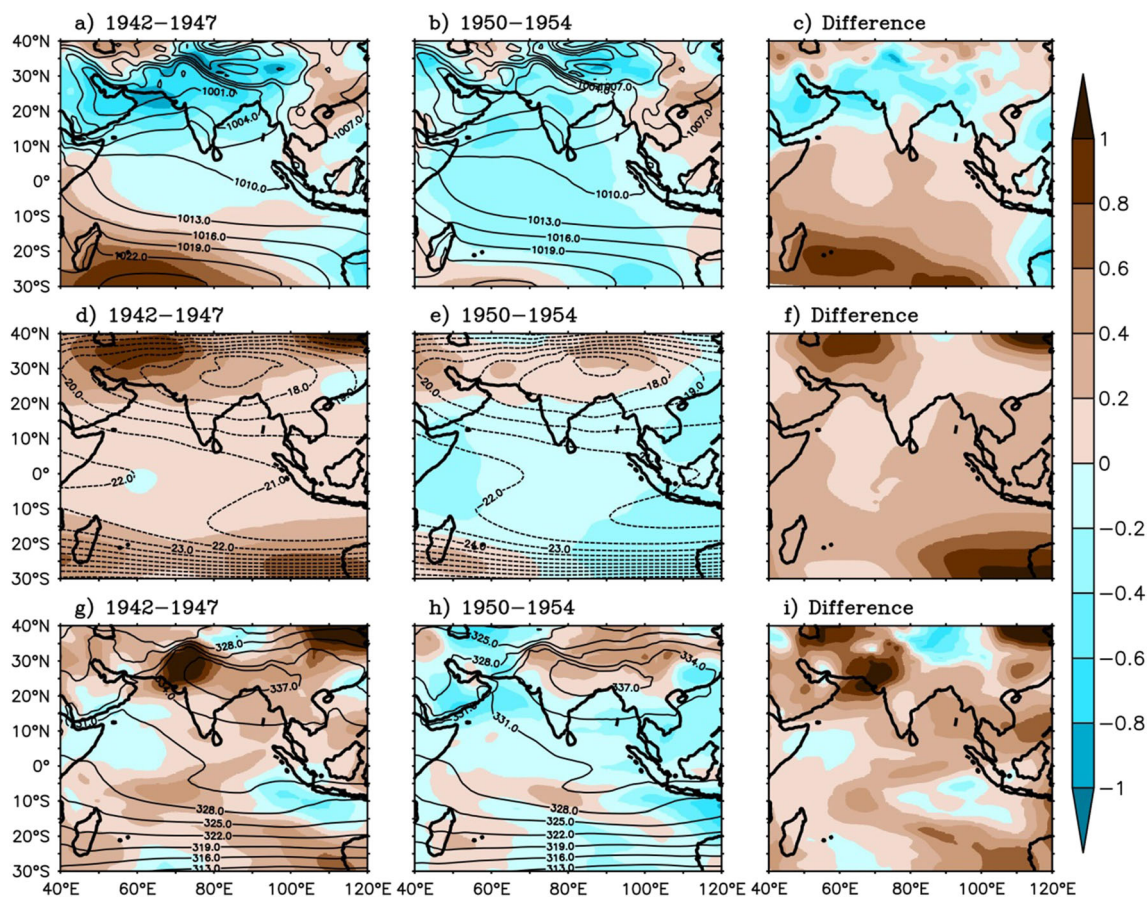


Fig. 6 Spatial pattern of JJAS mean sea level pressure (hPa, contour) and sea level pressure anomaly (hPa, shaded) for the warm (a) and cold phase (b) and their difference (c, a-b). Troposphere temperature (°C, average over the 600 to 200 hPa, contour) and its anomaly (°C, shaded), for the

warm phase (d) and cold phase (e) and their difference (f, d-e). Moist static energy (kJ/kg, average over the 1000 to 200 hPa, contour) and its anomaly (kJ/kg, shaded), for the warm phase (g) and cold phase (h) and their difference (i, g-h)

3.3 Zonal and meridional circulation during the warm and cold phase of TIO SST decadal variability

Observational and modeling studies have shown that decadal variability of TIO SST can influence the tropical and extra-tropical atmospheric circulation through changes in the zonal (Walker) and meridional (Hadley) circulations (Wang and Mehta 2008). Figure 7 shows the anomalous Walker and Hadley cell during the warm and cold phases of the dominant decadal variability of the TIO SST. The Walker cell circulation during the warm phase (Fig. 7(a)) averaged over the 18° N to 28° N, and shows upward circulation anomaly from 50° E to 110° E (except 75° E to 85° E), throughout the troposphere manifesting above-normal convection over this region, which is consistent with the strong convective activity in the TIO during the warm phase. During the cold phase (Fig. 7(b)), strong upward circulation anomaly is limited, and their vertical extent is also restricted, manifesting weaker convective activity. In Walker cell, strong convergence and updraft is reported around 60° E to 75° E, during the warm phase compared to the cold phase (Fig. 7(c)), which is coinciding with

the positive rainfall anomaly over the northwestern India; lower troposphere displayed strong anomalous westerly over the region 60° E to 90° E with the vertical extent up to 850 hPa and in the upper troposphere strong divergence is reported, manifesting strong monsoon state over 18° N to 28° N and 60° E to 90° E, which is part of MCZ. Overall, zonal circulation features are consistent with the monsoon features reported during the warm and cold phases. These circulation features indicate that monsoon circulation was stronger during the warm phase than the cold phase.

Figure 7(d) shows the anomalous Hadley cell during the warm phase averaged over 70 to 90° E. It shows upward vertical velocity anomaly for the 7° S to 35° N (except 15 to 20° N) throughout the troposphere. However, during the cold phase, mostly downward vertical velocity anomaly is reported; this manifests below-normal convective activity during the cold phase in the meridional section also. In addition to the above, the meridional cell during the warm and cold phases (Fig. 7(d-f)) clearly shows stronger southerly wind anomalies in the lower troposphere to 800 hPa in warm compared to cold phase and has strong convergence at 10° N and 30° N,

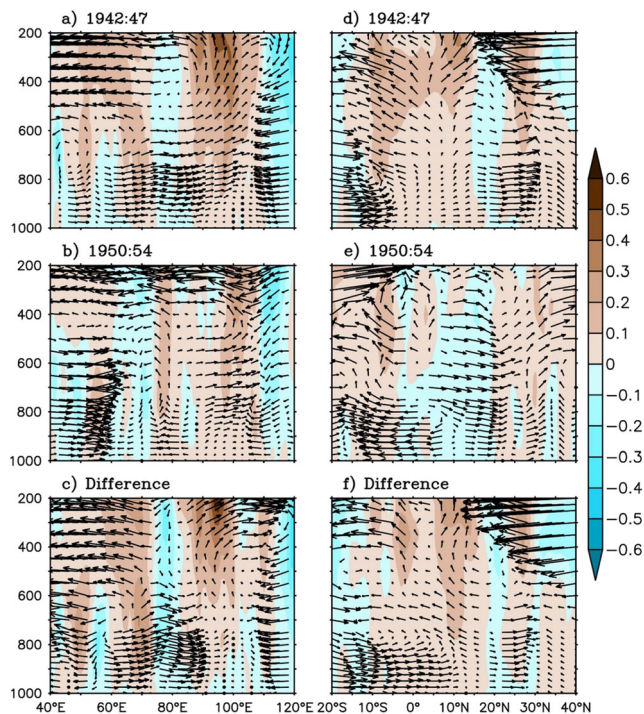


Fig. 7 Anomalous Walker cell circulation (vector u , $w \times 100$, latitude average between 18° N and 28° N) during the (a) warm phase, (b) cold phase, (c) difference (a–b), and anomalous Hadley cell circulation (vector, $w \times 100$ longitude average between 70° E and 90° E) during the (d) warm phase, (e) cold phase, and (f) difference (d–e). Shading is the corresponding vertical velocity anomaly (m/s) multiply by the 100

coinciding with strong upward draft. The northern convergence center is coinciding with the positive precipitation anomalies, consistent with the upper troposphere divergence. The above analysis reveals that zonal, as well as meridional circulation associated with the summer monsoon, does display coherent response to the TIO SST variability through in-phase monsoon variability. It also conveys that TIO SST variability at low-frequency scale influences three-dimensional monsoon circulation, affects moist thermodynamics and physics, and leads the monsoon variability at decadal scale.

3.4 Vertical structure of circulation and moist thermodynamics over the MCZ for the warm and cold phases of TIO SST decadal variability

As discussed earlier, MCZ displayed significant positive rainfall anomaly during the warm phase (Fig. 4(d, e)) and vice versa. Corresponding response of monsoon circulation and moisture are studied over the MCZ for the warm and cold phases, respectively (Fig. 8). Figure 8(a–c) displays wind anomaly for the warm and cold phases; in the warm phase, anomalous winds are positive up to the mid-troposphere and negative above, indicating stronger than normal monsoon flow. However, during the cold phase, anomalous winds are closer to the normal. Monsoon winds are baroclinic in nature

over the MCZ, westerly in the lower troposphere, and easterly in the upper troposphere, during the strong monsoon; in general, it has stronger winds and vice versa for the weaker monsoon. Figure 8(d) shows the vertical profile of specific humidity anomaly, which represents moisture over the MCZ during warm and cold phases. For the warm phase, whole troposphere displays positive anomaly, with noticeable magnitude in the lower to mid-troposphere (1000 to 400 hPa) and has maximum positive anomaly about 800 hPa, which might be due to the warm TIO SST, support evaporation, and supply of this excess moisture through monsoon circulation to the MCZ, favoring positive rainfall anomaly during the warm phase, whereas during the cold phase, weak anomalies are reported. Associated temperature anomaly (Fig. 8(e)) is negative in the lower troposphere for both the cases; however, mid-troposphere to upper troposphere temperature has noticeable difference for the warm and cold phases, which specifies that the contribution of diabatic heating to temperature structure over the MCZ is higher for the warm phase than the cold phase. Corresponding profile of MSE anomaly shows (Fig. 8(f)) positive anomaly throughout the troposphere in the warm phase, with maximum MSE anomaly at about 800 hPa, which is resembling with the moisture profile (Fig. 8(d)). Hence, the strongest MSE anomalies peak in the lower troposphere and are, primarily, regulated by advected moisture flux anomalies (Fig. 5(d–f)), whereas for the cold phase, it has negative anomaly in the lower troposphere (due to internal energy contribution) and weak positive anomaly in the mid-troposphere with maxima at 500 hPa. This analysis indicates that over the MCZ, excess moisture is supplied by the warm TIO, which gets uplifted by the monsoon-associated convergence and favors the excess monsoon rainfall. Over the MCZ relative to circulation, the moist thermodynamic displayed greater difference between the warm and cold phases.

4 Summary and conclusion

Tropical Indian Ocean (TIO) SST variations have large climate impacts both regionally and globally. Recent studies (e.g., Han et al. 2014b) have reported that like Pacific and Atlantic SST, TIO SST also has decadal variability, which has almost a basin-scale structure with the period of 9 to 30 years. Similarly, several studies reported that Indian summer monsoon rainfall (ISMR) has decadal variability (Kripalani and Kulkarni 1997a, b, Mehta and Lau 1997, Krishnamurthi and Goswami 2000) but the role of TIO SST for the ISMR variability is unclear, which has motivated us to carry out the present study using more than 100 years of SST, rainfall, and ERA20C reanalysis atmospheric data. Time series and wavelet analysis confirmed that significant (at 80%) decadal variability (~ 9 to 30 years) is present in the TIO SST. The variance of decadal variability of TIO SST is maximum in

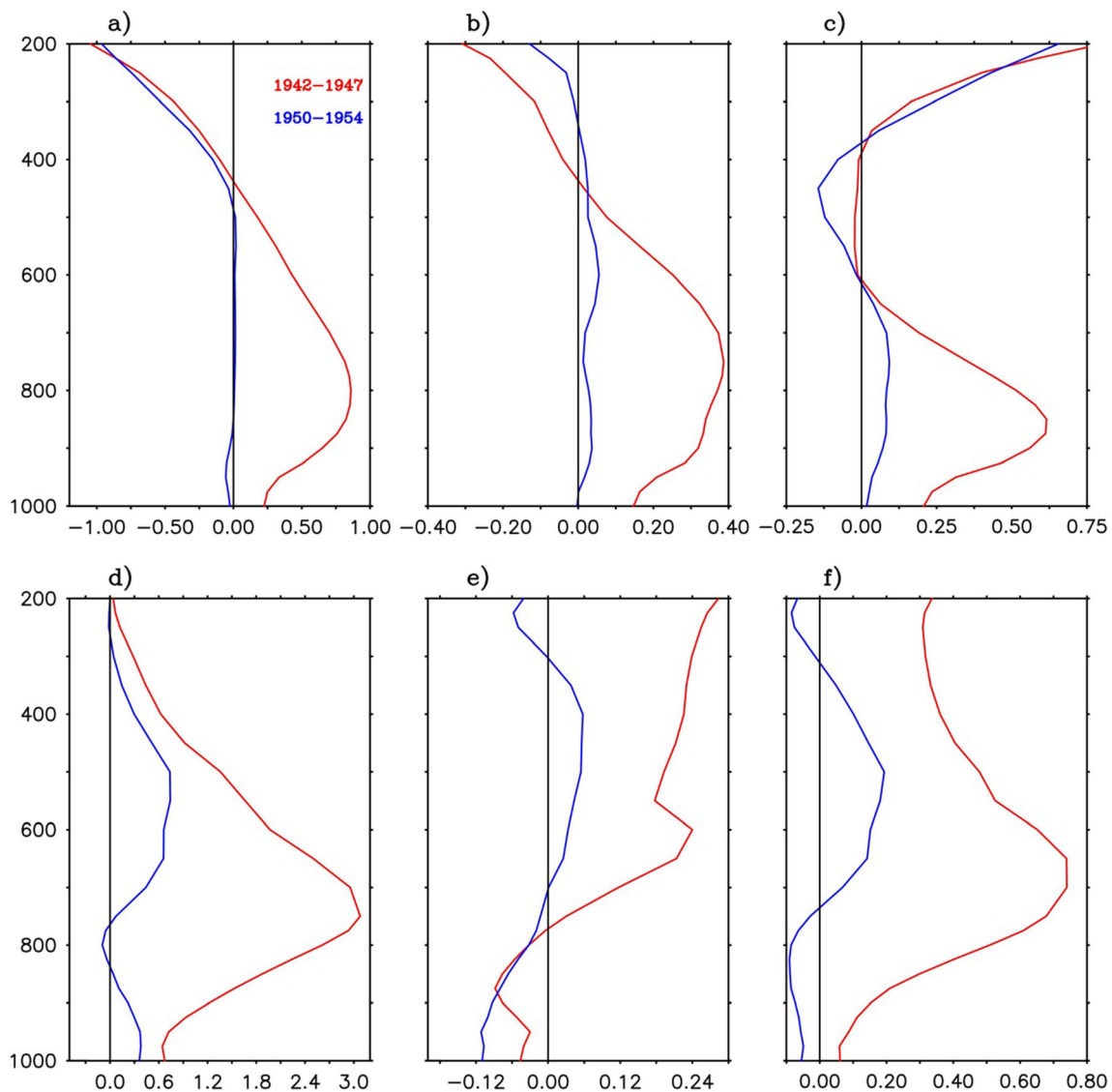


Fig. 8 Vertical profile averaged over the MCZ (72° E– 88° E; 18° N– 26° N) for anomaly of (a) zonal wind (ms^{-1}), (b) meridional wind (ms^{-1}), (c) wind speed anomaly (ms^{-1}), (d) specific humidity $\times 10^{-4}$, (e)

tropospheric temperature ($^{\circ}\text{C}$), (f) moist static energy (kJ kg^{-1}) for the warm phase (red line) and cold phase (blue line) respectively

the eastern equatorial Indian Ocean, followed by the north Arabian Sea. Decadal EOF of TIO SST shows basin-wide dominant mode explaining about 50% of total variance. Principal component of EOF analysis shows robust decadal variability during 1940 to 1952, having positive epoch during 1940 to 1945 (i.e., warm phase) and strongest negative epoch is during 1948 to 1952 (i.e., cold phase); wavelet analysis supported this robust signal statistically. Analysis also confirmed that TIO SST decadal variability strength is of the order of AMO strength. For the study period, correlation coefficient between decadal variability of TIO SST and AMO index is about 0.4, whereas between PDO and IPO is about 0.3, which are significant with the confidence level of 95%. The phase relation between decadal variability of TIO SST with PDO and IPO is found to vary with time. Similar spatial and

temporal analysis for the ISMR reveals that the strength of the ISMR decadal variability is meager; however, spatial pattern of variance of decadal rainfall variability over India shows that MCZ and Western Ghats have significant strength of the decadal variability. The EOF analysis further confirms this spatial pattern of rainfall decadal variability over India. Correlation analysis for Indian rainfall with decadal TIO SST shows that correlation is weaker for ISMR, but it is higher and significant for the MCZ rainfall with the lag of 2 years.

To understand how the decadal variability of TIO SST influences the summer monsoon features, monsoon features during warm and cold phase are studied. This analysis reveals that during the warm phase, MCZ and Western Ghats receive more rain than normal and vice versa during the cold phase. However, the rest of India does not show significant

differences during these two phases. The more rainfall over MCZ and Western Ghats during warm phase is consistent with strong southwesterly winds, strong-pressure gradient, and strong convergence over the MCZ and vice versa reported for the negative phase. Also, during the warm phase, positive mid-troposphere temperature anomaly is found over the north of 20° N, supporting excess convective activity, which is also reflected in the vertical velocity analysis and moist static energy. Apart from this, larger scale zonal (Walker) and meridional (Hadley) circulation fields are also in phase with the TIO SST and rainfall variability. This finding confirms that warm (cold) phase of TIO SST decadal variability favored positive (negative) rainfall anomaly over MCZ through air–sea interaction and monsoon dynamics. Thus, the present study reveals that warm phase supports stronger meridional gradient of surface pressure; leads to strong supply low-level moisture flux, convergence of it along the Western Ghats and MCZ; and results in more convection and associated tropospheric heating due to excess rainfall and vice versa during the cold phase with relatively less amplitude. However, it remained unclear how decadal variability of TIO SST gets influenced by variabilities such as AMO, PDO, and IPO through oceanic as well as atmospheric pathways and their contribution to reported monsoon features during the different phases. Apart from this, it is also not clear why such strong decadal variability in TIO SST is not reported during the recent period when monsoon displayed decadal variability. These are required to be explored in detail in the future studies.

Acknowledgments We acknowledge the Director of ESSO-IITM and Ministry of Earth Sciences, Government of India, for the support. We thank the anonymous reviewers for providing very insightful suggestions and critical comments for the improvement of the manuscript.

References

- Ajaymohan R, Rao SA (2008) Indian Ocean dipole modulates the number of extreme rainfall events over India in a warming environment. *J Meteorol Soc Jpn* 86(1):245–252. <https://doi.org/10.2151/jmsj.86.245>
- Allan RJ, Lindesay JA, Reason CJC (1995) Multidecadal variability in the climate system over the Indian Ocean region during austral summer. *J Climate* 8:1853–1873
- Annamalai H (2010) Moist dynamical linkage between the equatorial Indian Ocean and the South Asian monsoon trough. *J Atmos Sci* 67:589–610
- Ashok K, Le Chan W, Motoi T, Yamagata T (2004) Decadal variability of the Indian Ocean dipole. *Geophys Res Lett* 31(24):1–4. <https://doi.org/10.1029/2004GL021345>
- Bader J, Latif M (2005) North Atlantic oscillation response to anomalous Indian ocean SST in a coupled GCM. *J Clim* 18(24):5382–5389. <https://doi.org/10.1175/JCLI3577.1>
- Cassou C, Kushnir Y, Hawkins E, Pirani A, Kucharski F, Kang S, Caltabiano N (2018) Decadal climate variability and predictability: challenges and opportunities. *BAMS* 99(3):479–490
- Cherchi A, Navarra A (2013) Influence of ENSO and of the Indian Ocean dipole on the Indian summer monsoon variability. *Clim Dyn* 41(1): 81–103
- Dong L, McPhaden M (2016) Interhemispheric SST gradient trends in the Indian Ocean prior to and during the recent global warming hiatus. *J Clim* 29(24):9077–9095
- Dong L, McPhaden M (2017) Why has the relationship between Indian and Pacific Ocean decadal variability changed in recent decades? *J Climate* 30(6):1971–1983
- Dong L, Zhou T, Dai A, Song F, Wu B, Chen X (2016) The footprint of the inter-decadal Pacific oscillation in Indian Ocean Sea surface temperatures. *Sci Rep* 6:21251
- Fasullo J (2004) Biennial characteristics of Indian monsoon rainfall. *J Clim* 17:2972–2982
- Feng M, McPhaden MJ, Lee T (2010) Decadal variability of the Pacific subtropical cells and their influence on the Southeast Indian Ocean. *Geophys Res Lett* 37(9):1–6. <https://doi.org/10.1029/2010GL042796>
- Findlater J (1969) A major low-level air current near the Indian Ocean during the northern summer. *Quart J Roy Meteor Soc* 95:362–380
- Flohn H (1957) Large-scale aspects of the “summer monsoon” in South and East Asia. *J Meteor Soc Japan* 75:180–186
- Flohn H (1960) Recent investigation on the mechanism of the “summer monsoon” of southern and eastern Asia. *Monsoon of the world*. The Manager of Publications, Civil Lines, Delhi, India, 75–88
- Gadgil S, Rajeevan M, Francis PA (2007) Monsoon variability: links to major oscillations over the equatorial Pacific and Indian oceans. *Curr Sci* 93(2):182–194
- Goswami BN (2006) The Asian monsoon: interdecadal variability. In: *The Asian monsoon* (pp. 295–327). Springer, Berlin, Heidelberg
- Goswami BN, Venugopal V, Sengupta D, Madhusoodanan MS, Xavier PK (2006) Increasing trend of extreme rain events over India in a warming environment. *Science* 314(5804):1442–1445. <https://doi.org/10.1126/science.1132027>
- Han W, Meehl GA, Rajagopalan B, Fasullo JT, Hu A, Lin J et al (2010) Patterns of Indian Ocean sea-level change in a warming climate. *Nat Geosci* 3:546
- Han W, Meehl GA, Hu A, Alexander MA, Yamagata T, Yuan D et al (2014a) Intensification of decadal and multi-decadal sea level variability in the western tropical Pacific during recent decades. *Clim Dyn* 43(5–6):1357–1379. <https://doi.org/10.1007/s00382-013-1951-1>
- Han W, Vialard J, McPhaden MJ, Lee T, Masumoto Y, Feng M, de Ruijter WPM (2014b) Indian Ocean decadal variability: a review. *BAMS* 95(11):1679–1703. <https://doi.org/10.1175/bams-d-13-00028.1>
- Hawkins E, Sutton R (2009) The potential to narrow uncertainty in regional climate predictions. *BAMS* 90(8):1095–1108. <https://doi.org/10.1175/2009bams2607.1>
- Huang B, Banzon VF, Freeman E, Lawrimore J, Liu W, Peterson TC, Smith TM, Thorne PW, Woodruff SD, Zhang H-M (2014) Extended reconstructed sea surface temperature version 4 (ERSST.v4): part I. upgrades and inter comparisons. *J Climate* 28:911–930. <https://doi.org/10.1175/JCLI-D-14-00006.1>
- Huang B, Thorne P, Smith T, Liu W, Lawrimore J, Banzon V, Zhang H, Peterson T, Menne M (2015) Further exploring and quantifying uncertainties for extended reconstructed sea surface temperature (ERSST) version 4 (v4). *J Clim* 29:3119–3142. <https://doi.org/10.1175/JCLI-D-15-0430.1>
- Huang Y, Wu B, Li T, Zhou T, Liu B (2019) Interdecadal Indian Ocean Basin mode driven by interdecadal Pacific oscillation: a season-dependent growth mechanism. *J Climate* 32:2057–2073. <https://doi.org/10.1175/JCLI-D-18-0452.1>
- Izumo T, Lengaigne M, Vialard J, Luo JJ, Yamagata T, Madec G (2014) Influence of Indian Ocean dipole and Pacific recharge on following year’s El Niño: interdecadal robustness. *Clim Dyn* 42(1–2):291–310
- Kamae Y, Watanabe M, Kimoto M, Shioyama H (2014) Summertime land–sea thermal contrast and atmospheric circulation over East

- Asia in a warming climate—part I: past changes and future projections. *Clim Dyn* 43:2553–2568
- Konwar M, Parekh A, Goswami BN (2012) Dynamics of east-west asymmetry of Indian summer monsoon rainfall trends in recent decades. *Geophys Res Lett* 39(10):1–6. <https://doi.org/10.1029/2012GL052018>
- Koul V, Parekh A, Srinivas G, Kakatkar R, Chowdary JS, Gnanaseelan C (2018) Role of ocean initial conditions to diminish dry bias in the seasonal prediction of Indian summer monsoon rainfall: a case study using Climate Forecast System. *J Adv Model Earth Syst* 10:603–616. <https://doi.org/10.1002/2017MS001129>
- Kripalani, R. H., & Kulkarni, A. (1997a). Climatic impact of El Niño / La Niña on the Indian monsoon : weather, 52(2), 39–46. <https://doi.org/10.1002/j.1477-8696.1997.tb06267.x>
- Kripalani RH, Kulkarni A (1997b) Rainfall variability over South-East Asia - connections with Indian monsoon and Enso extremes: new perspectives. *Int J Climatol* 17(11):1155–1168. [https://doi.org/10.1002/\(SICI\)1097-0088\(199709\)17:11<1155::AID-JOC188>3.0.CO;2-B](https://doi.org/10.1002/(SICI)1097-0088(199709)17:11<1155::AID-JOC188>3.0.CO;2-B)
- Krishnamurthi V, Goswami BN (2000) Indian monsoon ENSO relationship on interdecadal timescale. *Am Meteorol Soc*:579–595
- Krishnamurthy L, Krishnamurthy V (2014) Influence of PDO on south Asian summer monsoon and monsoon-ENSO relation. *Clim Dyn* 42(9–10):2397–2410. <https://doi.org/10.1007/s00382-013-1856-z>
- Krishnamurthy L, Krishnamurthy V (2016) Decadal and interannual variability of the Indian Ocean SST. *Clim Dyn* 46(1–2):57–70. <https://doi.org/10.1007/s00382-015-2568-3>
- Krishnamurthy V, Shukla J (2008) Seasonal persistence and propagation of intraseasonal patterns over the Indian monsoon region. *Clim Dyn* 30(4):353–369. <https://doi.org/10.1007/s00382-007-0300-7>
- Krishnan R, Sugi M (2003) Pacific decadal oscillation and variability of the Indian summer monsoon rainfall. *Clim Dyn* 21(3–4):233–242. <https://doi.org/10.1007/s00382-003-0330-8>
- Kucharski F, Parvin A, Rodríguez-Fonseca B, Farneti R, Martín-Rey M, Polo I, Mohino E, Losada T, Mechoso CR (2016) The teleconnection of the tropical Atlantic to Indo-Pacific Sea surface temperatures on inter-annual to centennial time scales: a review of recent findings. *Atmosphere* 7(2):29
- Lee T, McPhaden MJ (2008) Decadal phase change in large-scale sea level and winds in the Indo-Pacific region at the end of the 20th century. *Geophys Res Lett* 35(1):1–7. <https://doi.org/10.1029/2007GL032419>
- Li Y, Han W (2015) Decadal Sea level variations in the Indian Ocean investigated with HYCOM: roles of climate modes, ocean internal variability, and stochastic wind forcing. *J Clim* 28(23):9143–9165. <https://doi.org/10.1175/JCLI-D-15-0252.1>
- Li Y, Jourdain NC, Taschetto AS, Ummenhofer CC, Ashok K, Sen Gupta A (2012) Evaluation of monsoon seasonality and the tropospheric biennial oscillation transitions in the CMIP models. *Geophys Res Lett* 39(20)
- Li G, Xie S-P, Du Y (2015a) Monsoon-induced biases of climate models over the tropical southeastern Indian Ocean. *J Clim* 28:3058–3072
- Li G, Xie S-P, Du Y (2015b) Climate model errors over the South Indian Ocean thermocline dome and their effect on the basin mode of interannual variability. *J Clim* 28:3093–3098
- Li G, Xie S-P, Du Y (2016a) A robust but spurious pattern of climate change in model projections over the tropical Indian Ocean. *J Clim* 29:5589–5608
- Li X, Xie S-P, Gille ST, Yoo C (2016b) Atlantic-induced pan-tropical climate change over the past three decades. *Nat Clim Chang* 6: 275–279. <https://doi.org/10.1038/nclimate2840>
- Li G, Xie S-P, He C, Chen Z (2017) Western Pacific emergent constraint lowers projected increase in Indian summer monsoon rainfall. *Nat Clim Chang* 7:708–712
- Lindzen RS, Nigam S (1987) On the role of sea surface temperature gradients in forcing low-level winds and convergence in the tropics. *J Atmos Sci* 44(17):2418–2436. [https://doi.org/10.1175/15200469\(1987\)044<2418:OTROSS>2.0.CO;2](https://doi.org/10.1175/15200469(1987)044<2418:OTROSS>2.0.CO;2)
- Liu X, Yanai M (2001) Relationship between the Indian monsoon rainfall and the tropospheric temperature over the Eurasian continent. *Q J R Meteorol Soc* 127(573):909–937. <https://doi.org/10.1256/smsqj.57310>
- Liu W, Huang B, Thorne PW, Banzon VF, Zhang H-M, Freeman E, Lawrimore J, Peterson TC, Smith TM, Woodruff SD (2014) Extended Reconstructed sea surface temperature version 4 (ERSST.v4): part II. Parametric and structural uncertainty estimations. *J Climate* 28:931–951. <https://doi.org/10.1175/JCLI-D-14-00007.1>
- Liu ZY (2012) Dynamics of interdecadal climate variability: A historical perspective. *J Clim* 25:1963–1995
- Luo J-J, Sasaki W, Masumoto Y (2012) Indian Ocean warming modulates Pacific climate change. *Proc Natl Acad Sci* 109(46):18701–18706. <https://doi.org/10.1073/pnas.1210239109>
- Maloney ED (2009) The moist static energy budget of a composite tropical intraseasonal oscillation in a climate model. *J Clim* 22:711–729
- Mandke S, Sahai AK, Shinde MA, Joseph S, Chatopadhyay R (2007) Simulated changes in active/break spells during the Indian summer monsoon due to enhanced CO₂ concentrations: assessment from selected coupled atmosphere–ocean global climate models. *Int J Climatol* 27:837–859
- Mantua NJ, Hare SR, Zhang Y, Wallace JM, Francis RC (1997) A Pacific interdecadal climate oscillation with I. *BAMS* 78(6)
- Meehl GA (1994) Coupled land-ocean-atmosphere processes and south Asian monsoon variability. *Science* 266(5183):263–267. <https://doi.org/10.1126/science.266.5183.263>
- Meehl GA, Goddard L, Murphy J, Stouffer RJ, Boer G, Danabasoglu G et al (2009) Decadal prediction. *BAMS* 90(10):1467–1486. <https://doi.org/10.1175/2009BAMS2778.1>
- Mehta V, Lau K (1997) Influence of solar irradiance on the Indian monsoon-ENSO relationship at decadal-multidecadal time scales. *Geophys Res Lett* 24(2):159–162
- Mohapatra S, Gnanaseelan C, Deepa JS (2020) Multidecadal to decadal variability in the equatorial Indian Ocean subsurface temperature and the forcing mechanisms. *Clim Dyn*:1–13. <https://doi.org/10.1007/s00382-020-05185-7>
- Mooley DA, Parthasarathy B (1984) Fluctuations in all India summer monsoon rainfall during 1871–1978. *Clim Chang* 6:287–301. <https://doi.org/10.1007/BF00142477>
- Nakamura H, Lin G, Yamagata T (1997) Decadal climate variability in the North Pacific during the recent decades. *BAMS* 78(10):2215–2225. [https://doi.org/10.1175/1520-0477\(1997\)078<2215:DCVITN>2.0.CO;2](https://doi.org/10.1175/1520-0477(1997)078<2215:DCVITN>2.0.CO;2)
- Pai DS, Sridhar L, Rajeevan M, Sreejith OP, Satbhai NS, Mukhopadhyay B (2014) Development of a new high spatial resolution (0.25°×0.25°) long period (1901–2010) daily gridded rainfall dataset over India and its comparison with existing datasets over the region. *Mausam* 65(1):1–18
- Pant G, Kumar K, Parthasarathy B, Borgaonkar H (1988) Long-term variability of the Indian summer monsoon and related parameters. *Adv Atmos Sci* 5(4):469–481
- Pattnayak KC, Panda SK, Vaishali S, Dash SK (2016) Relationship between tropospheric temperature and Indian summer monsoon rainfall as simulated by RegCM3. *Clim Dyn* 46:3149–3162
- Poli P, Hersbach H, Dee DP, Berrisford P, Simmons AJ, Vitart F, Laloyaux P, Tan DGH, Peubey C, Thépaut JN, Trémolet Y, Hólm EV, Bonavita M, Isaksen I, Fisher M (2016) ERA-20C: an atmospheric reanalysis of the twentieth century. *J Clim* 29(11):4083–4097. <https://doi.org/10.1175/JCLI-D-15-0556.1>
- Rajeevan M, Bhate J, Kale JD, Lal B (2006) A high-resolution daily gridded rainfall for the Indian region: analysis of break and active monsoon spells. *Curr Sci* 91:296–306

- Rajeevan M, Sulochana G, Jyoti B (2010) Active and break spells of the Indian summer monsoon. *J Earth Syst Sci* 119(3):229–247
- Rajeevan, M., C. K. Unnikrishnan, and B. Preethi (2012) Evaluation of the ENSEMBLES multi-model seasonal forecasts of Indian summer monsoon variability. *Climate Dynamics* 38.11–12 2257–2274
- Raju A, Parekh A, Chowdary JS, Gnanaseelan C (2018) Reanalysis of the Indian summer monsoon: four dimensional data assimilation of AIRS retrievals in a regional data assimilation and modeling framework. *Clim Dyn* 50(7–8):2905–2923. <https://doi.org/10.1007/s00382-017-3781-z>
- Roy SS, Sen Roy N (2011) Influence of Pacific decadal oscillation and El Niño southern oscillation on the summer monsoon precipitation in Myanmar. *Int J Climatol* 31(1):14–21. <https://doi.org/10.1002/joc.2065>
- Roy S, Goodrich GB, Balling RC (2003) Influence of El Niño/southern oscillation, Pacific decadal oscillation, and local sea-surface temperature anomalies on peak season monsoon precipitation in India. *Clim Res* 25(2):171–178. <https://doi.org/10.3354/cr025171>
- Salinger MJ, Renwick JA, Mullan AB (2001) Interdecadal Pacific oscillation and South Pacific climate. *Int J Climatol* 21(14):1705–1721
- Schlesinger ME, Ramankutty N (1994) An oscillation in the global climate system of period 65–70 years. *Nature* 367(6465):723–726. <https://doi.org/10.1038/367723a0>
- Sen Roy S (2011a) Identification of periodicity in the relationship between PDO, El Niño and peak monsoon rainfall in India using S-transform analysis. *Int J Climatol* 31:1507–1517
- Sen Roy S (2011b) The role of the North Atlantic oscillation in shaping regional scale peak seasonal precipitation across the Indian subcontinent. *Earth Interact* 15. <https://doi.org/10.1175/2010EI339.1>
- Su H, Neelin JD (2002) Teleconnection mechanism for tropical Pacific descent anomalies during El Niño. *J Atmos Sci* 59:2694–2712
- Torrence C, Compo G (1998) A practical guide to wavelet analysis. *BAMS* 79(1):61–78
- Torrence C, Webster PJ (1999) Interdecadal changes in the ENSO monsoon system. *J Clim* 12:2679–2690
- Tozuka T, Luo JJ, Masson S, Yamagata T (2007) Decadal modulations of the Indian Ocean dipole in the SINTEX-F1 coupled GCM. *J Clim* 20(13):2881–2894. <https://doi.org/10.1175/JCLI4168.1>
- Trenberth KE, Hurrell JW (1994) Decadal atmosphere-ocean variations in the Pacific. *Clim Dyn* 9:303. <https://doi.org/10.1007/BF00204745>
- Trenberth KE, Shea DJ (2006) Atlantic hurricanes and natural variability in 2005. *Geophys Res Lett* 33:L12704. <https://doi.org/10.1029/2006GL026894>
- Wang H, Mehta VM (2008) Decadal variability of the indo-Pacific warm Pool and its association with atmospheric and oceanic variability in the NCEP–NCAR and SODA reanalyses. *J Clim* 21(21):5545–5565. <https://doi.org/10.1175/2008JCLI2049.1>
- Xavier PK, Marzin C, Goswami BN (2007) An objective definition of the Indian summer monsoon season and a new perspective on the ENSO–monsoon relationship. *Q J R Meteorol Soc* 133:749–764
- Yan XH, Boyer T, Trenberth K, Karl TR, Xie SP, Nieves V, Tung KK, Roemmich D (2016) The global warming hiatus: slowdown or redistribution? *Earth's Future* 4(11):472–482. <https://doi.org/10.1002/2016EF000417>
- Yoo SH, Yang S, Ho CH (2006) Variability of the Indian Ocean Sea surface temperature and its impacts on Asian-Australian monsoon climate. *J Geophys Res Atmos* 111(D3)
- Zhou XM, Li SL, Luo F, Gao Y, Furevik T (2015) Air-sea coupling enhances east Asian winter climate response to the Atlantic multidecadal oscillation (AMO). *Adv Atmos Sci* 32:1647–1659. <https://doi.org/10.1007/s00376-015-5030-x>

Publisher's note Springer Nature remains neutral with regard to jurisdictional claims in published maps and institutional affiliations.